Infrared and Raman spectra, conformational stability, and ab initio calculations of cyclobutyl trifluorosilane

ARTICLE *in* JOURNAL OF MOLECULAR STRUCTURE · JANUARY 2000

Impact Factor: 1.6 · DOI: 10.1016/S0022-2860(99)00195-7

4 AUTHORS, INCLUDING:

Marwan Dakkouri
Universität Ulm
104 PUBLICATIONS **933** CITATIONS
SEE PROFILE

Todor K Gounev
University of Missouri - Kansas City
77 PUBLICATIONS **576** CITATIONS
SEE PROFILE

ELSEVIER

Journal of Molecular Structure 516 (2000) 161–175

Journal of
MOLECULAR
STRUCTURE

www.elsevier.nl/locate/molstruc

Infrared and Raman spectra, conformational stability, and ab initio calculations of cyclobutyl trifluorosilane ☆

J.R. Durig[a,*], M. Dakkouri[b], T.K. Gounev[a], P. Zhen[a]

[a]*Department of Chemistry, University of Missouri—Kansas City, Kansas City, MO 64110-2499, USA*
[b]*Abteilung für Elektrochemie, Universität Ulm, 89081 Ulm, Germany*

Received 8 March 1999; accepted 6 April 1999

Abstract

The infrared (3500–40 cm^{-1}) spectra of gaseous and solid and the Raman spectrum (3500–30 cm^{-1}) of liquid and solid cyclobutyl trifluorosilane, c-$C_4H_7SiF_3$, have been recorded. From the Raman spectrum of the liquid qualitative depolarization values have been obtained. Both the axial and equatorial conformers have been identified in the fluid phases. Variable temperature (−55 to −150°C) studies of the infrared spectra of the sample dissolved in liquid xenon and krypton have been carried out. From these data, the enthalpy difference has been determined to be 25 ± 10 cm^{-1} (0.30 ± 0.12 kJ/mol), with the equatorial conformer being the more stable form. A complete vibrational assignment is proposed for both conformers based on infrared band contours, relative intensities, depolarization values and group frequencies and the assignments are supported by normal coordinate calculations utilizing ab initio force constants. Complete equilibrium geometries have been determined for both rotamers by ab initio calculations employing different basis sets at the levels of restricted Hartree–Fock (RHF) and/or Moller–Plesset (MP) to second order. The results are discussed and compared to those obtained for some similar molecules.

Keywords: Infrared and Raman spectra; Conformational stability; Ab initio calculations; Cyclobutyl trifluorosilane

1. Introduction

Four-membered ring molecules have one low-frequency ring-puckering mode and the nature of the potential function governing this vibration determines the conformational stability of the ring. In the initial far infrared and low frequency Raman investigations [1,2] of methylcyclobutane, the spectroscopic studies addressed only the methyl torsional and ring puckering modes with little attention given to the remaining portion of the vibrational spectrum. These earlier results were consistent with the equatorial conformer energetically favored over the axial form. Additionally, it was inferred that a large value of the enthalpy difference, ΔH, between the two conformers should result in little or none of the high-energy axial form being present at ambient temperature. However, the more recent studies [3,4] of methylcyclobutane provided clear evidence that the value of ΔH for both the liquid and vapor phases was sufficiently small (<400 cm^{-1}) to allow for the direct observation of several of the vibrational modes of the high-energy axial conformation. Similarly for the halocyclobutane

☆ Taken, in part, from the dissertation of Pengqian Zhen, which will be submitted to the Department of Chemistry, University of Missouri—Kansas City, Kansas City, MO, in partial fulfillment of the PhD degree.

* Corresponding author. Tel.: +1-816-235-1136; fax: +1-816-235-5191.

E-mail address: durigi@umkc.edu (J.R. Durig).

0022-2860/00/$ - see front matter
PII: S0022-2860(99)00195-7

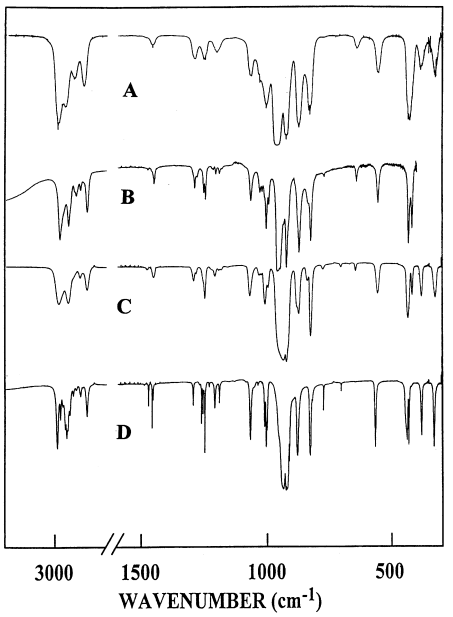

Fig. 1. Mid-infrared spectra of cyclobutyl trifluorosilane in the: (A) gas; (B) xenon solution at −80°C; (C) amorphous solid; and (D) annealed solid.

molecules [5–7], the enthalpy differences between the conformers have been found in the same general range (300–400 cm^{-1}) so that several fundamentals from the axial conformers have been identified.

The infrared and Raman spectra of gaseous and solid as well as the Raman spectrum of liquid cyclobutylsilane, c-$C_4H_7SiH_3$ have been investigated [8]. From a comparison of the spectra of the fluid phases with that of the solid, it has been shown that two stable conformers exist in the fluid phases at ambient temperature. It was determined that the equatorial conformer is the predominant form at ambient temperature in the gas phase and, from a temperature study of the Raman spectrum in this phase, the enthalpy difference between the equatorial and axial conformers was determined to be 147 ± 50 cm^{-1} (1.76 ± 0.60 kJ/mol). Similar studies of the Raman spectrum of the liquid phase gave an enthalpy difference of 231 ± 25 cm^{-1} (2.76 ± 0.30 kJ/mol), again with the equatorial conformer being thermodynamically preferred and the only conformer present in the solid state.

A series of Q-branches obtained from the low frequency Raman and far infrared spectra of gaseous cyclobutyl silane as well as sum and difference bands in the 1600–1200 cm^{-1} region were assigned to the ring puckering vibration of both the low-energy equatorial and high-energy axial conformers and fitted to an asymmetric potential function of the form $V(cm^{-1}) = (3.13 \pm 0.09) \times 10^5 X^4 + (1.36 \pm 0.04) \times 10^4 X^3 - (2.30 \pm 0.08) \times 10^4 X^2$. This potential is consistent with the equatorial conformation being more stable than the axial by 188 cm^{-1} (2.25 kJ/mol), and the equatorial to axial barrier is 531 cm^{-1} (6.35 kJ/mol). From this potential function puckering angles of 21.3 and 17.8° were obtained for the equatorial and axial conformers, respectively.

As a continuation of these studies, we initiated an infrared and Raman spectroscopic study of cyclobutyl trifluorosilane, c-$C_4H_7SiF_3$, to determine the presence or absence of conformers at ambient temperature and, if they are present, to determine their relative stabilities. As an aid in interpreting the vibrational spectra, we have carried out ab initio calculations at the RHF/6-31G*, MP2/6-31G* and MP2/6-311++G** levels. The optimized geometries, conformational stabilities, harmonic force fields, infrared intensities, Raman activities, depolarization ratios, and vibrational frequencies have been obtained to compare with the experimental results where applicable. The results of these spectroscopic and theoretical studies are reported herein.

2. Experimental

Various attempts have been undertaken to prepare cyclobutyl trifluorosilane in high yields and purity [9], and it turned out that the most efficient and easiest way of preparation is the following one. A sample of cyclobutyl trichlorosilane was prepared by the treatment of cyclobutyl-Grignard and silicon tetrachloride analogously to the preparation of cyclobutyl trichlorogermane according to the route which was described previously [10]. The cyclobutyl trichlorosilane was then transformed to cyclobutyl trifluorosilane by direct fluorination with anhydrous ZnF_2. The sample was initially purified by using a spinning-band column fractionation (b.p. 52°C/707 Torr) and further was purified with a low-temperature, low-pressure fractionation column. Complete details of the preparation and purification will be given elsewhere [9].

The mid-infrared spectra of the gas and solid (Fig. 1) were obtained from 3500 to 300 cm^{-1} on a Perkin–Elmer model 2000 Fourier transform spectrometer equipped with a Ge/CsI beam-splitter and a DTGS detector. The gas was contained in a 10 cm cell fitted with CsI windows. This spectrum was obtained at 0.5 cm^{-1} resolution and transformed with boxcar truncation function. The spectrum of the solid was obtained by condensing the sample onto a liquid nitrogen cooled CsI plate contained in an evacuated cell equipped with CsI windows, and 256 scans were collected for both the reference and sample interferograms at 1 cm^{-1} resolution and then transformed with a boxcar truncation function.

The mid-infrared spectra of the sample dissolved in liquified xenon (Fig. 1(B)) and krypton (Fig. 2(A)) as a function of temperature were recorded on a Bruker model IFS 66 Fourier transform spectrometer equipped with a globar source, a Ge/KBr beam-splitter and a DTGS detector. In xenon solution, we collected the spectra from −55 to −100°C, and in krypton from −105 to −150°C. In all cases, 100 interferograms were collected at 1.0 cm^{-1} resolution, averaged and transformed with a boxcar truncation function. For these studies, a specially designed cryostat cell was used. It consisted of a copper cell with a pathlength of 4 cm with wedged silicon windows sealed to the cell with indium gaskets. The copper cell was enclosed in an evacuated chamber fitted with KBr windows. The temperature was maintained with boiling liquid nitrogen and monitored with two Pt thermoresistors. The complete cell was connected to a pressure manifold, allowing the filling and evacuation of the system. After cooling to the desired temperature, a small amount of the compound was condensed into the cell. Next, the system was pressurized with the noble gas, which immediately started to condense in the cell, allowing the compound to dissolve.

The far infrared spectrum of cyclobutyl trifluorosilane in the vapor phase (Fig. 3(A)) was recorded with a Nicolet model 200 SXV vacuum Fourier transform interferometer. The instrument was fitted with a vacuum bench, 6.25 μm Mylar beam-splitter and a liquid helium cooled Ge bolometer detector. The interferometer was evacuated to 1 Torr. An average of 512 interferograms were Fourier transformed using the Happ–Genzel apodization function and a theoretical resolution of 0.12 cm^{-1}. The sample was dried with 3 Å molecular sieves and contained in a 1 m optical path cell. The far infrared spectra of the amorphous (Fig. 3(B)) and crystalline solids (Fig. 3(C)) were obtained with the Perkin–Elmer model 2000 spectrometer equipped with a metal grid beam-splitter and a DTGS detector.

The Raman spectra (Fig. 4) were recorded on a SPEX model 1403 spectrophotometer equipped with a Spectra-Physics model 164 argon ion laser operating on the 514.5 nm line. The laser power used was 0.5 W with a spectral bandpass of 3 cm^{-1}. The spectrum of the liquid was recorded with the sample sealed in a Pyrex glass capillary held in a Miller–Harney apparatus [11]. Depolarization measurements were obtained for the liquid sample using a standard Ednalite 35 mm camera polarizer with 38 mm of free aperture affixed to the SPEX instrument. Depolarization ratio measurements were checked by measuring the state of polarization of the Raman bands of CCl_4 immediately before depolarization measurements were made on the liquid sample. The Raman frequencies are expected to be accurate to $\pm$ 2 cm^{-1}. The Raman spectrum of the solid was obtained by cooling the sample capillary with chilled nitrogen vapors until the sample solidified. All of the observed bands in both the infrared and Raman spectra, along with the proposed assignments are listed in Table 1.

3. Ab initio calculations

The LCAO-MO-SCF restricted Hartree–Fock calculations were performed with the GAUSSIAN 94 program [12] using Gaussian-type basis functions. The energy minima with respect to nuclear coordinates were obtained by the simultaneous relaxation of all of the geometric parameters consistent with the symmetry restrictions using the gradient method of Pulay [13]. The 6-31G* and/or 6-311++G** basis sets were employed at the level of restricted Hartree–Fock (RHF) and Moller–Plesset (MP2) to second order [14]. The determined structural parameters are listed in Table 2.

In order to obtain a more complete description of the molecular motions involved in the normal modes of cyclobutyl trifluorosilane (Fig. 5), we have carried out a normal coordinate analysis. The force fields in

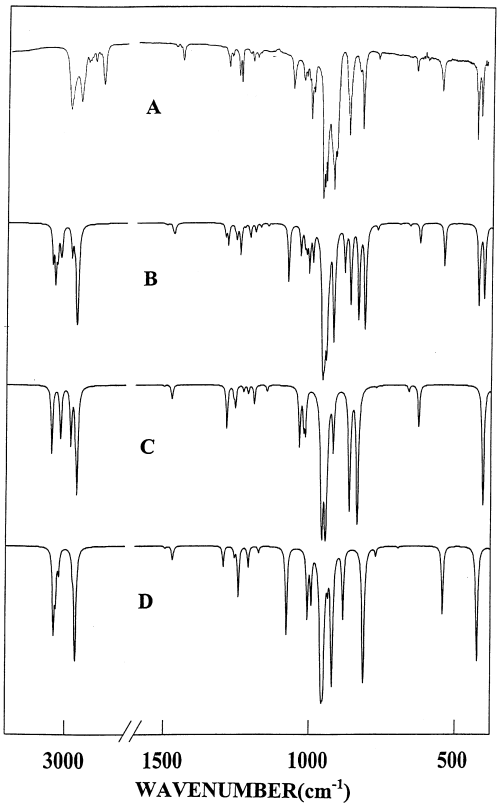

Fig. 2. Mid-infrared spectra of cyclobutyl trifluorosilane: (A) krypton solutions at −125°C; (B) calculated spectrum of the mixture of both conformers; (C) calculated spectrum of the axial conformer; and (D) calculated spectrum of the equatorial conformer.

Cartesian coordinates were calculated by the GAUSSIAN 94 program [12] with the MP2/6-31G* basis set. The internal coordinates listed in Table 2 were used to calculate the **G** and **B** matrices utilizing the structural parameters obtained from the MP2/6-31G* calculation. Using the **B** matrix [15], the force field in Cartesian coordinates was then converted to a force field in internal coordinates, and the pure ab initio vibrational frequencies were reproduced. The force constants for both the axial and equatorial conformers can be obtained from the authors. Subsequently, scaling factors of 0.9 for stretching and bending and 1.0 for the torsional coordinate, and the geometric average of scaling factors for interaction force constants were used to obtain the fixed scaled force field and resultant wavenumbers. A set of symmetry coordinates (Table 3) was used to determine the corresponding potential energy distributions (PED).

To aid in the vibrational assignment, Raman and infrared spectra for cyclobutyl trifluorosilane were calculated using the predicted frequencies, scattering activities and intensities determined from the ab initio calculations. The evaluation of Raman activities by using the analytical gradient methods has been previously developed [16,17]. The activity S_j can be expressed as:

$$S_j = g_j(45\alpha_j^2 + 7\beta_j^2)$$

where g_j is the degeneracy of the vibrational mode j, α_j is the derivative of the isotropic polarizability, and β_j is that of the anisotropic polarizability. The Raman scattering cross-sections, $\partial\sigma_j/\partial\Omega$, which are proportional to the Raman intensities, can be calculated from the scattering activities and the predicted wavenumbers for each normal mode using the relationship [18,19]:

$$\frac{\partial\sigma_j}{\partial\Omega} = \left(\frac{2^4\pi^4}{45}\right)\left(\frac{(\nu_0-\nu_j)^4}{1-\exp[-\mathrm{hc}\nu_j/\mathrm{k}T]}\right)\left(\frac{\mathrm{h}}{8\pi^2\mathrm{c}\nu_j}\right)S_j$$

where ν_0 is the exciting frequency, ν_j is the vibrational frequency of the jth normal mode, h, c and k are universal constants, and S_j is the corresponding Raman scattering activity. To obtain the polarized Raman scattering cross section, the polarizabilities are incorporated into S_j by $S_j[(1-\rho_j)/1+\rho_j]$ where ρ_j is the depolarization ratio of the jth normal mode. The Raman scattering cross sections and calculated fixed scaled frequencies are used together with a Lorentzian line shape function to obtain the calculated spectrum. The predicted Raman spectra of the pure axial and equatorial conformers are shown in Fig. 6(C) and (D), respectively. The predicted Raman spectrum of the mixture of the two conformers with an assumed ΔH of 25 cm^{-1} is shown in Fig. 6(B) which should be compared to the experimental spectrum of the liquid (Fig. 6(A)). The ΔH value utilized is the value obtained from the temperature dependent study of the spectra from the xenon and krypton solutions and the agreement between the observed and calculated spectra is satisfactory.

Infrared intensities were also calculated based on the dipole moment derivatives with respect to the Cartesian coordinates. The derivatives were taken

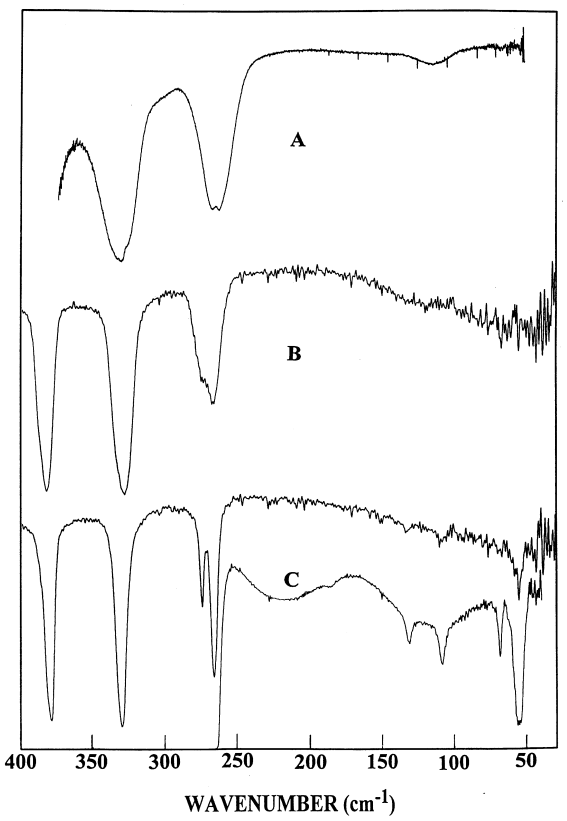

Fig. 3. Far infrared spectra of cyclobutyl trifluorosilane in the: (A) gas; (B) amorphous solid; and (C) annealed solid.

from the ab initio calculations at the MP2/6-31G* level and transformed to normal coordinates by:

$$\left(\frac{\partial \mu_u}{\partial Q_i}\right) = \sum_j \left(\frac{\partial \mu_u}{\partial X_j}\right) \mathbf{L}_{ij}$$

where Q_i is the ith normal coordinate, X_j is the jth Cartesian displacement coordinate, and $\mathbf{L}_{ij}$ is the transformation matrix between the Cartesian displacement coordinates and normal coordinates. The infrared intensities were then calculated by

$$I_i = \frac{N\pi}{3c^2}\left[\left(\frac{\partial \mu_x}{\partial Q_i}\right)^2 + \left(\frac{\partial \mu_y}{\partial Q_i}\right)^2 + \left(\frac{\partial \mu_z}{\partial Q_i}\right)^2\right].$$

In Fig. 2(C) and (D), the predicted infrared spectra of the axial and equatorial conformers, respectively, are shown. The combination of the spectra of the two conformers with a ΔH of 25 cm^{-1} is shown in Fig. 2(B) and the experimental spectrum of the sample dissolved in liquid krypton is shown in Fig. 2(A). A comparison between the observed and calculated frequencies of cyclobutyl trifluorosilane along with the calculated infrared intensities, Raman activities, depolarization ratios and PED are given in Table 4.

4. Conformational stability

There are several examples in both the Raman and infrared spectra, which show that there is more than one conformer of cyclobutyl trifluorosilane present in the fluid phases. For example, the polarized band at 645 cm^{-1} in the Raman spectrum of the liquid completely disappears in the Raman spectrum of the polycrystalline solid (Fig. 4). In the infrared spectra (Fig. 1) of the gas, bands at 644 and 431 cm^{-1} remain in the spectrum of the amorphous solid but disappear upon crystallization of the sample. These bands are confidently assigned to the fundamentals of the axial conformer since the ab initio calculations clearly show that these bands are due to this conformer. Also, these data clearly indicate that the equatorial conformer is the only form present in the polycrystalline solid.

The conformer pairs at 556/643 and 433/420 cm^{-1} (Fig. 7) were used to determine the enthalpy difference between the conformers by the temperature dependent infrared spectra of xenon and krypton solutions. Twenty sets of spectral data were obtained for these bands over the temperature range −55 to −100°C for xenon and from −105 to −150°C for krypton (Table 5). The intensity data for the conformer bands were fit to the van't Hoff equation $-\ln K = (\Delta H/RT) - (\Delta S/R)$, where K is substituted with the intensity ratio (I_{eq}/I_{ax}), and it is assumed that ΔH is not a function of temperature. Using a least-squares fit and the slope of the van't Hoff plot, an average ΔH value of 25 ± 10 cm^{-1} (0.30 ± 0.12 kJ/mol) was obtained with the equatorial conformer being more stable. This value should be representative for ΔH in the gas phase [20–24], since the molecular sizes and dipole moments of both conformers are almost the same.

5. Vibrational assignment

Both the axial and equatorial conformers of

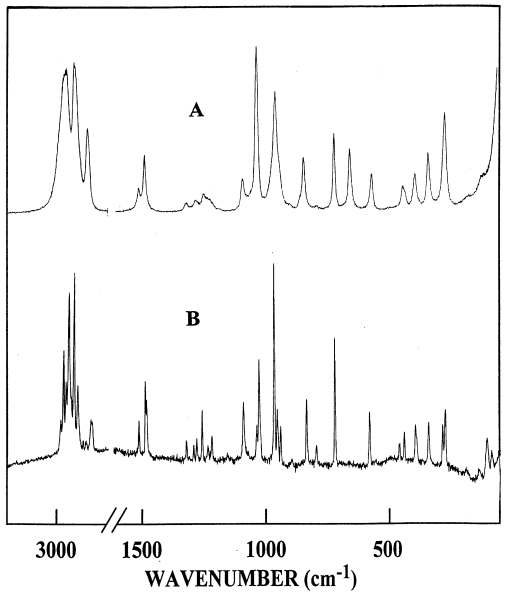

Fig. 4. Raman spectra of cyclobutyl trifluorosilane in the: (A) liquid; and (B) annealed solid.

cyclobutyl trifluorosilane have a plane of symmetry and the 39 normal modes span the representations of 23 A' and 16 A'' species of the C_s symmetry group. The A' vibrations are expected to produce polarized Raman lines and A, C and A/C-type hybrid infrared band contours. The A'' modes should give rise to depolarized lines in the Raman spectrum and yield B-type infrared band envelopes. Thus, to identify the A' and A'' vibrations, we utilized the measured depolarization ratios and observed infrared band contours, whereas to distinguish between the equivalent modes of the two conformers we relied on the predicted wavenumber order, infrared intensities, and Raman activities from the ab initio calculations.

There are six expected CH_2 stretching fundamentals and three CH_2 deformational modes of cyclobutyl trifluorosilane. There are five pronounced bands in the infrared spectrum located in the C–H stretching region. They are assigned according to the ab initio predictions with the lowest frequency band at 2886 cm^{-1} assigned as an overtone in Fermi resonance with the stretching fundamental. The CH_2 deformations are attributed to the pair of bands at 1476 and 1452 cm^{-1} in the Raman spectrum of the liquid. The CH stretches of the equatorial and axial conformers are assigned at 2957 and 2925 cm^{-1}, respectively, whereas the CH in-plane bends of the two conformers are observed as weak bands at 1289 and 1284 cm^{-1}, respectively.

The separation of the fundamentals of the two conformers becomes more apparent below 1300 cm^{-1}, especially in the infrared spectrum of the Xe and Kr solutions where the spectral bands are much sharper than the corresponding ones of the gas or liquid. For example, the CH in-plane bends of the equatorial and axial conformers are observed at 1284 and 1275 cm^{-1} in the spectrum of the Xe solution. The band centered at 1249 cm^{-1} in the Raman spectrum of the liquid is associated with the three wagging modes of the CH_2 groups, whereas two of the CH_2 twisting vibrations are located at 1202 and 1180 cm^{-1} for the equatorial conformer (Raman data) and 1212 and 1188 for the axial form in the infrared spectrum of the Xe solution. The other CH_2 twisting mode is assigned at 993 cm^{-1} for the equatorial conformer and at 1019 cm^{-1} for the axial conformer.

The A' $(CH_2)_2$ rocking mode of the axial conformer which is expected around 1030 cm^{-1} is obscured by a low boiling point impurity band which exhibits a sharp double Q-branch at 1031/1030 cm^{-1} in the infrared spectrum of the gas. The respective fundamental of the equatorial form is observed at 1069 cm^{-1} in the same spectrum. The other two CH_2 rocking modes are observed at 876 and 779 cm^{-1} for the equatorial conformer.

A cluster of very strong bands is observed in the infrared spectrum between 900 and 1000 cm^{-1} and these bands are associated with the various CC ring stretches and SiF_3 antisymmetric stretches. The C-type Q-branch at 1005 cm^{-1} is assigned to one of the A' C–C ring stretches whereas the other one is overlapped with the A'' C–C ring stretch and produces the pair of bands at 922 and 914 cm^{-1} for the equatorial and axial conformers, respectively, in the spectrum of the Xe solution.

The C–Si stretch is observed at 707 cm^{-1} for the equatorial conformer and the corresponding mode for the axial form is at 645 cm^{-1}. The ring deformation is assigned at 556 cm^{-1} for the equatorial conformer and the corresponding mode for the axial form is obscured by the C–Si stretching mode for this rotamer. The SiF_3 deformations are observed at 437, 329 and 264 cm^{-1} for the equatorial form and one of the

Table 1
Observed infrared and Raman wavenumbers (cm^{-1}) for cyclobutyl trifluorosilane (abbreviations used: s, strong; m, moderate; w, weak; v, very; bd, broad; sh, shoulder; p, polarized; dp, depolarized; ctr, center; A, B, and C refer to infrared band envelopes; P, Q, and R refer to the rotational–vibrational branches)

Infrared						Raman				Assignment	
Gas	Rel. int.	Xenon solution	Rel. int.	Solid	Rel. int.	Liquid	Rel. int. and depol.	Solid	Rel. int.	ν_i[a]	Approximate description
2996 R											
2991 Q	s			2992	s			2994	w		
2987 P	s	2982	s	2980	m	2987	sh,s,p	2983	s	ν_1, ν'_2	$(CH_2)_2$ antisymmetric stretch
2976 Q	sh	2976	sh,m	2971	w	2971	vs,p	2974	m	ν_{24}	$(CH_2)_2$ antisymmetric stretch
		2967	sh,m	2961	m	2963	vs,p	2963	vs	ν_2, ν'_1, ν'_{24}	CH_2 antisymmetric stretch
		2947	m							ν'_4	
2957 Q	s	2941	sh,m	2955	m			2943	vs	ν_3	C–H stretch
2952 P				2950	m						
2930 R											
2925 Q	w	2923	w	2927	w	2929	vs,p	2928	m	ν_4, ν'_3	CH_2 symmetric stretch
2919 P		2917	w	2916	vw	2920	sh,s,p	2922	sh,w	ν_5, ν_{25}	$(CH_2)_2$ symmetric stretches
		2911	sh,w							ν'_{25}	
		2900	w	2899	w			2906	vw		
2886	m	2888	w	2890	vw			2895	vw		
		2873	m	2873	m	2878	m,p	2875	w		
1476	sh,vw	1470	vw	1474	w	1476	w,p	1474	m	ν_6, ν'_6	$(CH_2)_2$ deformation
1457 Q	vw	1455	sh,vw							ν'_7	
1452 Q	vw	1446	w	1450	m	1452	m,dp	1449	s	ν_7, ν_{26}, ν'_{26}	CH_2 deformations
1448 Q	vw			1445	w			1444	m		
1294 R											
1289 Q	w	1284	w	1288	w	1288	vw,p	1288	w	ν_8	C–H in-plane bend
1284	w	1275	w							ν'_8	
				1255	m						
1250	bd,w	1249	w	1249	m			1258	vw	ν_{27}, ν'_9	CH_2 wag
1245 Q	w	1242	w	1241	s	1249	vw,p	1246	w	ν_9, ν_{28}	$(CH_2)_2$ wag
1244 Q	w										
1240 R											
1211	sh,w	1215	vw	1225	vw	1219	vw,dp	1225	m	ν_{29}	C–H out-of-plane bend
1207	w	1212	vw							ν'_{30}	
1200	w	1202	vw	1202	w	1202	sh,vw,p	1202	vw	ν_{10}	$(CH_2)_2$ twist
1192 Q	w	1188	vw			1195	sh,vw,p			ν'_{10}	
		1177	vw	1184	w	1180	sh,vw,dp	1186	w	ν_{30}	CH_2 twist
1073 R											
1069 Q	m	1062	w	1061	m	1065	w,p	1062	m	ν_{11}	$(CH_2)_2$ rock
1062 P											
1035 R											
1031 Q	m	1028	w			1031	sh,vw,p			ν'_{11}	$(CH_2)_2$ rock and impurity
1030 Q	m										

Table 1 (*continued*)

Infrared						Raman				Assignment	
Gas	Rel. int.	Xenon solution	Rel. int.	Solid	Rel. int.	Liquid	Rel. int. and depol.	Solid	Rel. int.	ν_i[a]	Approximate description
		1019	w							ν'_{31}	
		1009	sh,w			1009	vs,p			ν'_{12}	
1005 Q,C	s	1003	m	1006	m			1010	w	ν_{12}	C–C ring stretch
998	sh,vs	993	w	999	s			1001	s	ν_{31}	$(CH_2)_2$ twist
				996	m						
960 ctr	bd vs	959	vs	951	sh,m	953	sh,m,dp	942	vs	ν_{32}, ν'_{32}	SiF_3 antisymmetric stretch
		947	vs	931	vs	937	s,p	930	m	ν_{13}, ν'_{13}	SiF_3 antisymmetric stretch
		934	m							ν_{33}	C–C ring stretch
929 R											
925 Q	vs	922	vs	920 vs				917	w	ν_{14}, ν_{34}	C–C ring stretches
921 P				916	vs						
		914	sh,m	907	s					ν'_{14}, ν'_{34}	
880 R											
876 Q	s	879	sh,w	874	s	879	vw,p	874	vw	ν_{15}	CH_2 rock
875 Q	s	872	s							ν'_{15}	
870 P											
		837	w							ν'_{16}	
835 R											
831 Q	s	826	s	824	s	827	m,p	816	m	ν_{16}	SiF_3 symmetric stretch
826 P											
779	vw	775	w	772	m	776	vw,dp	777	vw	ν_{35}	$(CH_2)_2$ rock
		703	vw	701	w	707	m,p	705	vs	ν_{17}	C–Si stretch
648 R											
644 Q	vw	644	w			645	m,p			ν'_{17}	
560 R											
556 Q	w	556	w	562	s	559	w,p	567	m	ν_{18}	ring deformation
440 R				436	m			447	w		
437 Q	s	433	s	429	s	435	w,p	428	w	ν_{19}	SiF_3 symmetric deformation
431	s	420	m			425	sh,w,p			ν'_{19}	
389 Q	w									ν'_{36}	
380	sh,w			378	m	387	w,dp	384	w	ν_{36}	SiF_2 rock
329 max	w			329	s	332	m,p	332	m	ν_{20}, ν'_{20}	SiF_3 antisymmetric deformation
				273	w	267	s,p	277	m	ν_{21}, ν'_{23}	ring puckering
260 R											
264 min,B	w			265	m			266	m	ν_{37}, ν'_{37}	SiF_3 antisymmetric deformation
260 P											
				217	m					ν_{22}	SiF_3 rock
160	sh,vw					174	vw,p			ν'_{22}	

Table 1 (*continued*)

Infrared						Raman				Assignment	
Gas	Rel. int.	Xenon solution	Rel. int.	Solid	Rel. int.	Liquid	Rel. int. and depol.	Solid	Rel. int.	ν_i[a]	Approximate description
112	vw			132	vw	113	w,dp	134	vw	ν_{38}, ν'_{38}, ν_{23}	C–Si out-of-plane bend, C–Si in-plane bend
				108	vw			101	w		lattice modes
				69	vw			84	w		
				56	w			57	w		

[a] ν_i and ν_i' refer to the equatorial and axial conformers, respectively.

Table 2
Structural parameters (bond distances in Å, bond angles in degrees, rotational constants in MHz, dipole moments in Debye, and energies in Hartrees.), rotational constants, dipole moments, and energy for cyclobutyl trifluorosilane

Parameter	Internal coordinates	RHF/6-31G*		MP2/6-31G*		MP2/6-311++G**	
		Equatorial	Axial	Equatorial	Axial	Equatorial	Axial
$C_1-C_2(C_3)$	R_1,R_2	1.559	1.561	1.557	1.558	1.562	1.563
C_1-Si	R_5	1.844	1.844	1.832	1.834	1.830	1.832
C_1-H_{11}	r_7	1.087	1.086	1.095	1.096	1.095	1.095
$C_4-C_2(C_3)$	R_3,R_4	1.542	1.543	1.541	1.541	1.546	1.547
C_2-H_7	r_1	1.083	1.084	1.093	1.094	1.094	1.093
C_2-H_8	r_2	1.085	1.084	1.095	1.094	1.092	1.093
C_3-H_9	r_3	1.083	1.084	1.093	1.094	1.094	1.093
C_3-H_{10}	r_4	1.085	1.084	1.095	1.094	1.092	1.093
C_4-H_5	r_5	1.084	1.083	1.094	1.093	1.092	1.092
C_4-H_6	r_6	1.084	1.083	1.093	1.092	1.094	1.092
$Si-F_{13}$	r_8	1.577	1.577	1.601	1.601	1.602	1.602
$Si-F_{14}(F_{15})$	r_9,r_{10}	1.576	1.576	1.600	1.600	1.601	1.600
$\angle C_2C_1C_3$	θ_1	87.77	87.93	87.16	87.40	87.10	87.41
$\angle C_2C_4C_3$	ν_1	88.98	89.23	88.28	88.55	88.23	88.55
$\angle C_1C_2(C_3)C_4$	α_1,β_1	88.64	89.06	88.09	88.53	87.88	88.45
$\angle H_{11}C_1Si$	θ_2	109.7	108.4	111.6	108.9	110.7	108.0
$\angle H_5C_4H_6$	ν_6	108.7	108.7	108.9	109.0	109.6	109.3
$\angle H_7C_2H_8$	α_4	108.6	108.1	108.9	108.3	109.4	108.9
$\angle H_9C_3H_{10}$	β_4	108.6	108.1	108.9	108.3	109.4	108.9
$\angle C_1SiF_{13}$	λ_1	110.8	111.5	109.3	111.3	110.5	112.3
$\angle C_1SiF_{14}(F_{15})$	λ_2,λ_3	112.5	112.1	112.9	112.0	112.8	112.0
$\angle F_{13}SiF_{14}(F_{15})$	σ_3,σ_2	106.9	106.9	107.2	107.0	106.7	106.5
$\angle F_{14}SiF_{15}$	σ_1	106.9	107.0	107.1	107.2	107.0	107.2
$\angle H_6C_4C_2(C_3)$	ν_3, ν_5	111.6	117.2	110.9	117.9	110.5	117.9
$\angle H_5C_4C_2(C_3)$	ν_2, ν_4	117.5	111.7	118.3	111.1	118.3	111.0
$\angle C_4C_2(C_3)H_7(H_9)$	α_5,β_5	111.7	117.3	111.0	118.1	110.7	118.1
$\angle C_4C_2(C_3)H_8(H_{10})$	α_6,β_6	117.9	112.3	118.7	111.7	118.7	111.5
$\angle C_1C_2(C_3)H_7(H_9)$	α_2,β_2	112.3	118.3	111.2	118.8	111.2	118.8
$\angle C_1C_2(C_3)H_8(H_{10})$	α_3,β_3	116.8	110.9	117.5	110.2	117.4	109.9
$\angle SiC_1C_2(C_3)$	φ_1,φ_2	119.0	115.0	118.0	113.8	119.1	114.7
$\angle H_{11}C_1C_2(C_3)$	δ_1,δ_2	109.8	114.9	109.8	115.9	109.3	115.7
Puckering angle		25.99	23.11	30.75	28.11	31.71	28.39
$\tau(H_{11}C_1SiF_{13})$	τ	180.0	180.0	180.0	180.0	180.0	180.0
A		3006	2866	2958	2797	2953	2792
B		1127	1237	1133	1261	1120	1247
C		1049	1164	1054	1189	1043	1176
$\lvert\mu_a\rvert$		2.811	2.630	2.910	2.708	3.364	3.140
$\lvert\mu_b\rvert$		0.000	0.000	0.000	0.000	0.000	0.000
$\lvert\mu_c\rvert$		0.712	0.993	0.787	1.068	0.816	1.175
$\lvert\mu_t\rvert$		2.900	2.811	3.015	2.911	3.462	3.353
$-(E+740)$		2.97497	2.97418	4.13176	4.13145	4.67106	4.67067
ΔE (cm^{-1})			173		69		87

SiF_3 rocks is assigned at 380 cm^{-1} with the other one at 217 cm^{-1}. The ring puckering mode is assigned at 267 cm^{-1} but it contributes only 19% to this band with contributions of 46% to the 217 cm^{-1} band and 13% to the 112 cm^{-1} band which is assigned to the C–Si in-plane bend. Therefore, these low wavenumber bends are extensively mixed.

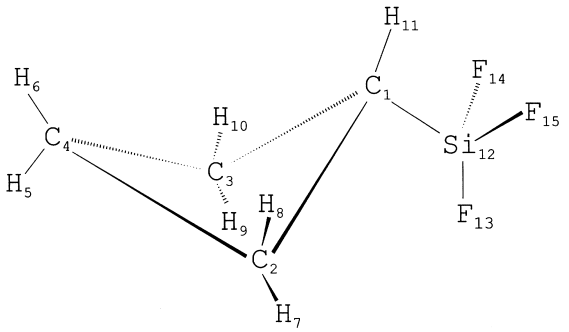

Fig. 5. Equatorial conformation of cyclobutyl trifluorosilane.

6. Results and discussion

The enthalpy differences (Table 5) were derived from the temperature dependent measurements in liquified xenon and krypton by using the intensity of two pairs of conformer bands. From the xenon solution using the 556/420 cm^{-1} pair, the enthalpy difference is $-3 \pm 4\ cm^{-1}$, and from the krypton solution this pair gives $+3 \pm 12\ cm^{-1}$. Another pair at 433/420 cm^{-1} gives $68 \pm 10\ cm^{-1}$ in the krypton solution. The average of these three values is $25 \pm 10\ cm^{-1}$, which indicates that the equatorial conformer is the more stable form in the rare gas solutions. Although the enthalpy value $25 \pm 10\ cm^{-1}$ is slightly lower than the ab initio predicted value of 69 cm^{-1} (MP2/6-31G* basis set), the predicted infrared spectrum (Fig. 2(B)) shows very good agreement with the observed spectrum (Fig. 2(A)) in the region below 1500 cm^{-1}, with some minor discrepancies. For example, there are four well defined fundamentals in the calculated infrared spectrum (Fig. 2(B)) at 884, 866, 837 and 826 cm^{-1}. The former two fundamentals are overlapped in the band at 872 cm^{-1} observed in the infrared spectrum of the krypton solution which makes the intensity of this band significantly larger than the prediction for either of the two fundamentals. The latter two fundamentals are also extensively overlapped in the same spectrum (Fig. 2(A)) at 837 and 826 cm^{-1} as the first band appears to have much lower intensity than the prediction. On the other hand, the various C–C ring stretches, ν_{14} and ν_{34}, of the two conformers are predicted to be almost coincident (Table 4); however, they appear as a very strong band and a shoulder at 922 and 914 cm^{-1} for the fundamentals of the equatorial and axial rotamers, respectively.

It is useful to compare the enthalpy differences between the conformers of cyclobutyl trifluorosilane, cyclobutylsilane [8] and methylcyclobutane [3]. These enthalpy differences increase in the above order from 25 ± 10 to 147 ± 50 to $295 \pm 75\ cm^{-1}$ with the equatorial conformer being more stable in all cases. Obviously, the axial conformation is greatly stabilized with respect to the equatorial when the CH_3 group is substituted by a SiH_3 or SiF_3 groups. The stability trend, however, cannot be explained based on the size of the substituent, because larger substituents (SiH_3 and SiF_3) should favor the equatorial conformer. MP2/6-31G* structural optimizations performed in this study showed that the puckering angles for the axial conformers of the three molecules are almost the same, ranging from 28.1 to 27.3°. Similarly, for the equatorial forms they range from 30.8 to 30.4°. Thus, we believe that the reason for the stabilization of the axial conformer is in the much longer C–Si distances of the C–SiF_3 and C–SiH_3 fragments compared to the C–C distance of the C–CH_3 fragment. These longer distances provide a greater separation between the in-plane atoms of the substituent (atom numbers 12 and 13 in Fig. 5) and the in-plane atoms of the ring (atom numbers 4 and 5 in Fig. 5) for the axial conformation. For example, the $H_{13}\cdots H_5$ distance for c-$C_4H_7SiH_3$ is 2.648 Å, which is about 0.2 Å longer than the distance in c-$C_4H_7CH_3$ (2.440 Å). Similarly, the $H_{13}\cdots C_4$ distances of these two molecules are 3.234 and 2.830 Å, respectively, a difference of 0.4 Å. The greater distance between the ring and the substituent should relieve the spatial restrictions in the axial form and, thus, lower its energy. The smaller conformational enthalpy difference of c-$C_4H_7SiF_3$ compared to c-$C_4H_7SiH_3$ can be attributed to the favorable interactions between the F_{13} and H_5 atoms (Fig. 5) in the axial conformer. The total atomic charges of these atoms as calculated with the MP2/6-31G* basis set are −0.49 and +0.19, respectively. For c-$C_4H_7SiH_3$, the corresponding atomic charges are only −0.15 and +0.17 for the atoms H_{13} and H_5.

The assignment of the C–H stretching modes must

Table 3
Symmetry coordinates for cyclobutyl trifluorosilane

Species	Description	Symmetry coordinate[a]
A′	$(CH_2)_2$ antisymmetric stretch	$S_1 = r_2 - r_1 + r_4 - r_3$
	CH_2 antisymmetric stretch	$S_2 = r_5 - r_6$
	C–H stretch	$S_3 = r_7$
	CH_2 symmetric stretch	$S_4 = r_5 + r_6$
	$(CH_2)_2$ symmetric stretch	$S_5 = r_1 + r_2 + r_3 + r_4$
	$(CH_2)_2$ deformation	$S_6 = 4\alpha_4 + 4\beta_4 - \alpha_2 - \alpha_3 - \alpha_5 - \alpha_6 - \beta_2 - \beta_3 - \beta_5 - \beta_6$
	CH_2 deformation	$S_7 = 4\nu_6 - \nu_2 - \nu_3 - \nu_4 - \nu_5$
	C–H in-plane bend	$S_8 = 2\theta_2 - \delta_1 - \delta_2$
	$(CH_2)_2$ wag	$S_9 = \alpha_2 + \alpha_3 - \alpha_5 - \alpha_6 + \beta_2 + \beta_3 - \beta_5 - \beta_6$
	$(CH_2)_2$ twist	$S_{10} = \alpha_2 - \alpha_3 - \alpha_5 + \alpha_6 + \beta_2 - \beta_3 - \beta_5 + \beta_6$
	$(CH_2)_2$ rock	$S_{11} = \alpha_2 - \alpha_3 + \alpha_5 - \alpha_6 + \beta_2 - \beta_3 + \beta_5 - \beta_6$
	C–C ring stretch	$S_{12} = R_1 + R_2 + R_3 + R_4$
	SiF_3 antisymmetric stretch	$S_{13} = 2r_8 - r_9 - r_{10}$
	C–C ring stretch	$S_{14} = R_1 + R_2 - R_3 - R_4$
	CH_2 rock	$S_{15} = \nu_3 - \nu_2 + \nu_5 - \nu_4$
	SiF_3 symmetric stretch	$S_{16} = r_8 + r_9 + r_{10}$
	C–Si stretch	$S_{17} = R_5$
	Ring deformation	$S_{18} = \alpha_1 + \beta_1 - \nu_1 - \theta_1$
	SiF_3 symmetric deformation	$S_{19} = \sigma_1 + \sigma_2 + \sigma_3 - \lambda_1 - \lambda_2 - \lambda_3$
	SiF_3 antisymmetric deformation	$S_{20} = 2\sigma_1 - \sigma_2 - \sigma_3$
	Ring puckering	$S_{21} = \alpha_1 + \beta_1 + \nu_1 + \theta_1$
	SiF_3 rock	$S_{22} = 2\lambda_1 - \lambda_2 - \lambda_3$
	C–Si in-plane bend	$S_{23} = \varphi_1 + \varphi_2$
A″	$(CH_2)_2$ antisymmetric stretch	$S_{24} = r_2 - r_1 + r_3 - r_4$
	$(CH_2)_2$ symmetric stretch	$S_{25} = r_1 + r_2 - r_3 - r_4$
	$(CH_2)_2$ deformation	$S_{26} = 4\alpha_4 - \alpha_2 - \alpha_3 - \alpha_5 - \alpha_6 - 4\beta_4 + \beta_2 + \beta_3 + \beta_5 + \beta_6$
	CH_2 wag	$S_{27} = \nu_4 + \nu_5 - \nu_2 - \nu_3$
	$(CH_2)_2$ wag	$S_{28} = \alpha_5 + \alpha_6 - \alpha_2 - \alpha_3 + \beta_2 + \beta_3 - \beta_5 - \beta_6$
	C–H out-of-plane bend	$S_{29} = \delta_1 - \delta_2$
	CH_2 twist	$S_{30} = \nu_2 - \nu_3 - \nu_4 + \nu_5$
	$(CH_2)_2$ twist	$S_{31} = \alpha_3 - \alpha_2 + \alpha_5 - \alpha_6 + \beta_2 - \beta_3 - \beta_5 + \beta_6$
	SiF_3 antisymmetric stretch	$S_{32} = r_9 - r_{10}$
	C–C ring stretch	$S_{33} = R_1 - R_2 - R_3 + R_4$
	C–C ring stretch	$S_{34} = R_1 - R_2 + R_3 - R_4$
	$(CH_2)_2$ rock	$S_{35} = \alpha_3 - \alpha_2 - \alpha_5 + \alpha_6 + \beta_2 - \beta_3 + \beta_5 - \beta_6$
	SiF_3 rock	$S_{36} = \lambda_2 - \lambda_3$
	SiF_3 antisymmetric deformation	$S_{37} = \sigma_3 - \sigma_2$
	C–Si out-of-plane bend	$S_{38} = \varphi_1 - \varphi_2$
	SiF_3 torsion	$S_{39} = \tau$

[a] Not normalized.

be considered somewhat tentative since selective deuteration of the β- and γ-CH_2 groups of the ring was not carried out. In general, the assignment follows that given earlier for the corresponding modes of the 1-methylsilacyclobutane [25] molecule where the assignments were made mainly on the basis of the ab initio predicted frequencies. In many cases the same or nearly the same wavenumbers are assigned for the corresponding modes for the two conformers. There are only a limited number of bands which could readily be assigned to the high energy axial conformer.

The potential energy distributions are extensively mixed for the A′ vibrational modes particularly those from ν_8 to ν_{23} except ν_{13} for the equatorial conformer. Some fundamentals cannot be appropriately described by the name which we have listed because they contain almost equal distributions of several modes,

Table 4
Observed and calculated frequencies (cm^{-1}) for equatorial and axial cyclobutyl trifluorosilane

Species	Vib. no.	Description	Equatorial							Axial						
			Ab initio[a]	Fixed scaled[b]	IR int.[c]	Raman act.[d]	dp ratio[d]	Obs.[e]	PED[f]	Ab initio[a]	Fixed scaled[b]	IR int.[c]	Raman act.[d]	dp ratio[d]	Obs.[e]	PED[f]
A′	ν^1	$(CH_2)_2$ antisymmetric stretch	3202	3038	36.2	54.7	0.59	2982	$61S_1,37S_2$	3180	3017	16.6	65.0	0.75	2967	$87S_1,12S_2$
	ν_2	CH_2 antisymmetric stretch	3185	3021	7.6	101.0	0.26	2967	$61S_2,33S_1$	3211	3047	26.5	54.3	0.60	2982	$87S_2,11S_1$
	ν_3	C–H stretch	3136	2975	5.5	184.7	0.08	2941	$86S_3$	3129	2968	10.5	76.4	0.32	2923	$68S_3,30S_5$
	ν_4	CH_2 symmetric stretch	3127	2967	16.4	54.7	0.73	2923	$64S_4,25S_5$	3144	2983	21.6	230.4	0.03	2947	$97S_4$
	ν_5	$(CH_2)_2$ symmetric stretch	3126	2965	14.7	88.7	0.37	2917	$57S_5,34S_4$	3121	2961	5.2	63.9	0.74	2911	$68S_5,31S_3$
	ν_6	$(CH_2)_2$ deformation	1577	1496	0.8	5.8	0.74	1470	$71S_6,27S_7$	1583	1502	0.4	7.6	0.72	1470	$72S_6,26S_7$
	ν_7	CH_2 deformation	1550	1471	4.1	18.7	0.75	1446	$72S_7,27S_8$	1556	1476	3.7	17.1	0.75	1455	$73S_7,27S_6$
	ν_8	C–H in-plane bend	1365	1295	6.7	3.3	0.73	1284	$29S_8,41S_9,17S_{10}$	1355	1286	15.2	1.7	0.73	1275	$33S_8,29S_9,22S_{10}$
	ν_9	$(CH_2)_2$ wag	1310	1243	16.2	5.9	0.68	1242	$46S_9,26S_8$	1324	1256	6.9	3.4	0.67	1249	$57S_9,15S_{10}$
	ν_{10}	$(CH_2)_2$ twist	1275	1209	6.8	8.4	0.72	1202	$52S_{10},16S_{17},10S_{11}$	1255	1191	6.0	7.6	0.73	1188	$37S_{10},23S_{15},16S_{11},13S_8$
	ν_{11}	$(CH_2)_2$ rock	1135	1077	38.4	11.0	0.08	1063	$29S_{11},30S_{12}$	1091	1035	22.4	19.1	0.11	1028	$32S_{11},35S_8$
	ν_{12}	C–C ring stretch	1060	1006	27.4	8.8	0.11	1003	$46S_{12},21S_8,11S_{11}$	1070	1015	15.0	11.0	0.19	1009	$50S_{12},34S_{14}$
	ν_{13}	SiF_3 antisymmetric stretch	1004	952	115.5	6.4	0.23	954	$75S_{13}$	996	945	158.2	2.0	0.67	947	$85S_{13}$
	ν_{14}	C–C ring stretch	971	921	95.4	2.0	0.16	922	$36S_{14},15S_{17},13S_{13}$	969	919	23.2	0.8	0.04	914	$45S_{14},21S_{12}$
	ν_{15}	CH_2 rock	932	884	28.3	1.4	0.67	879	$22S_{15},30S_{18},13S_{11},11S_{16}$	911	864	73.2	0.7	0.75	872	$25S_{15},25S_{18},23S_{16}$
	ν_{16}	SiF_3 symmetric stretch	859	815	91.4	3.3	0.12	826	$55S_{16},13S_{15},12S_{14}$	883	837	96.7	4.1	0.39	937	$49S_{16},17S_{18}$
	ν_{17}	C–Si stretch	733	696	0.6	4.8	0.07	707	$15S_{17},27S_{15},15S_{18},14S_{16}$	662	628	14.5	5.7	0.04	644	$35S_{17},16S_{16},16S_{11},13S_{18}$
	ν_{18}	Ring deformation	573	544	26.7	2.8	0.21	556	$38S_{18},18S_{17},15S_{11}$	697	662	2.1	1.7	0.51	–	$35S_{18},23S_{15},14S_{17}$
	ν_{19}	SiF_3 symmetric deformation	448	425	60.4	0.6	0.40	433	$43S_{19},21S_{23},13S_{22}$	428	406	66.5	0.4	0.42	420	$55S_{19},16S_{23}$
	ν_{20}	SiF_3 antisymmetric deformation	329	312	22.0	1.2	0.31	329	$62S_{20},22S_{19}$	334	317	23.8	0.7	0.29	329	$62S_{20},21S_{19}$
	ν_{21}	Ring puckering	271	257	12.1	1.2	0.37	(267)	$19S_{21},23S_{19},21S_{20},17S_{17},10S_{23}$	192	182	0.1	0.2	0.60	–	$58S_{21},24S_{22}$
	ν_{22}	SiF_3 rock	217	206	0.1	0.3	0.38	(217)	$37S_{22},46S_{21},10S_{20}$	145	138	1.0	0.0	0.75	160	$47S_{22},53S_{23}$
	ν_{23}	C–Si in-plane bend	108	103	0.8	0.1	0.46	112	$52S_{23},34S_{22},13S_{21}$	268	254	7.4	1.3	0.30	(267)	$11S_{23},24S_{21},23S_{20},16S_{19},11S_{17}$
A″	ν_{24}	$(CH_2)_2$ antisymmetric stretch	3195	3031	17.4	92.2	0.75	2976	$97S_{24}$	3183	3020	4.8	97.4	0.75	2967	$100S_{24}$
	ν_{25}	$(CH_2)_2$ symmetric stretch	3126	2965	34.0	3.2	0.75	2917	$97S_{25}$	3122	2962	48.3	0.7	0.75	2911	$100S_{25}$
	ν_{26}	$(CH_2)_2$ deformation	1546	1466	1.0	4.2	0.75	1446	$100S_{26}$	1553	1473	1.4	4.6	0.75	1446	$100S_{26}$
	ν_{27}	CH_2 wag	1325	1257	2.9	1.0	0.75	1249	$67S_{27}$	1330	1262	2.8	0.0	0.75	–	$70S_{27}$
	ν_{28}	$(CH_2)_2$ wag	1311	1243	2.1	0.5	0.75	1242	$55S_{28},20S_{29},14S_{31}$	1295	1228	1.9	0.4	0.75	–	$62S_{28},23S_{30},11S_{27}$
	ν_{29}	C–H out-of-plane bend	1283	1217	0.2	8.3	0.75	1215	$43S_{29},23S_{30},12S_{27}$	1209	1147	2.0	1.5	0.75	1149	$33S_{29},30S_{31},10S_{28},10S_{33}$
	ν_{30}	CH_2 twist	1236	1173	2.1	5.6	0.75	1177	$28S_{30},31S_{28},23S_{31}$	1277	1212	2.5	13.1	0.75	1212	$27S_{30},39S_{29},18S_{28},10S_{34}$
	ν_{31}	$(CH_2)_2$ twist	1046	993	19.0	6.0	0.75	993	$38S_{31},15S_{34},14S_{33},12S_{29},13S_{30}$	1076	1021	12.8	3.1	0.75	1019	$51S_{31},14S_{30},12S_{35},10S_{29}$
	ν_{32}	SiF_3 antisymmetric stretch	1009	957	148.5	0.2	0.75	959	$91S_{32}$	1009	957	149.8	0.1	0.75	959	$94S_{32}$
	ν_{33}	C–C ring stretch	987	936	8.1	17.3	0.75	934	$73S_{33}$	991	940	9.6	20.8	0.75	934	$79S_{33}$
	ν_{34}	C–C ring stretch	969	920	2.2	0.5	0.75	922	$60S_{34},11S_{29}$	964	914	0.4	0.3	0.75	914	$56S_{34},14S_{35},10S_{29}$
	ν_{35}	$(CH_2)_2$ rock	815	773	2.7	0.4	0.75	775	$77S_{35},11S_{30}$	814	773	0.5	0.1	0.75	775	$61S_{35},19S_{34},13S_{30}$
	ν_{36}	SiF_3 rock	386	367	15.8	1.2	0.75	380	$30S_{36},38S_{37},22S_{38}$	391	371	16.2	1.1	0.75	389	$31S_{36},36S_{37},26S_{38}$
	ν_{37}	SiF_3 antisymmetric deformation	268	255	3.1	0.4	0.75	264	$61S_{37},20S_{38},17S_{36}$	269	255	2.9	0.4	0.75	264	$63S_{37},19S_{38},17S_{36}$
	ν_{38}	C–Si out-of-plane bend	111	106	0.5	0.1	0.75	112	$52S_{38},44S_{36}$	118	112	0.5	0.0	0.75	112	$52S_{38},48S_{39}$
	ν_{39}	SiF_3 torsion	44	45	0.1	0.0	0.75	–	$95S_{39}$	16	16	0.0	0.0	0.75	–	$99S_{39}$

[a] Calculated with the MP2/6-31G* basis set.

[b] Scaling factors of 0.9 for stretching and bending coordinates and 1.0 for torsional coordinates.

[c] Calculated infrared intensities in km/mol.

[d] Calculated Raman activities in $Å^4$/amu, using RHF/6-31G* basis set.

[e] Frequencies are taken from the infrared spectrum of the gas, except the ones in parentheses, which are taken from the infrared spectrum of the solid or Raman spectrum of the liquid.

[f] For a description of the symmetric coordinates see Table 3.

Table 5
Temperature and intensity ratio for the conformational study of cyclobutyl trifluorosilane (average $\Delta H = 25 \pm 10\ cm^{-1}$ with the equatorial conformer more stable)

T (°C)	1000/T/K	$K = I_{556(eq)}/I_{643(ax)}$	$-\ln k$	$K = I_{556(eq)}/I_{643(ax)}$	$-\ln k$	$K = I_{433(eq)}/I_{420(ax)}$	$-\ln k$
−60	4.69	4.5500	−1.5151				
−65	4.80	4.5680	−1.5191				
−70	4.92	4.5700	−1.5195				
−75	5.05	4.5725	−1.5201				
−85	5.31	4.6189	−1.5302				
−90	5.46	4.5794	−1.5216				
−100	5.78	4.5641	−1.5182				
−110	6.13			4.8942	−1.5881		
−115	6.32			5.2637	−1.6608	2.0434	−0.7146
−120	6.53			4.9410	−1.5976	2.1148	−0.7490
−125	6.75			5.1496	−1.6389	2.1063	−0.7449
−130	6.99			4.8884	−1.5869	2.1310	−0.7566
−135	7.24			4.9864	−1.6067	2.3006	−0.8332
−140	7.51			4.8778	−1.5847	2.2828	−0.8254
−145	7.80			5.2443	−1.6571	2.4452	−0.8941
−150	8.12			4.9091	−1.5911	2.3823	−0.8681
ΔH (cm^{-1})			−3 ± 4		3 ± 12		68 ± 10

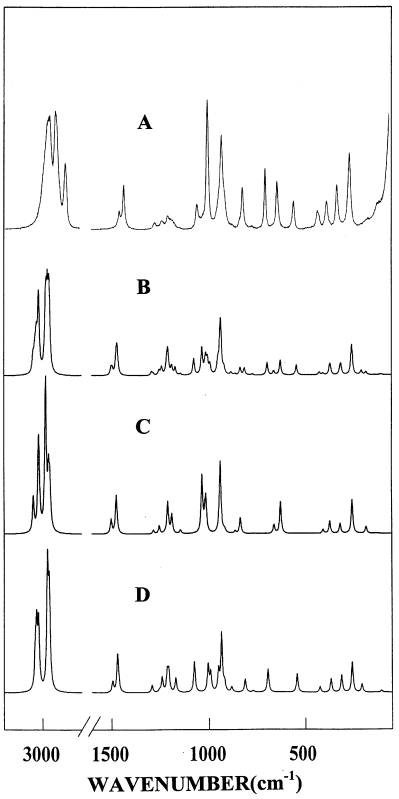

Fig. 6. Raman spectra of cyclobutyl trifluorosilane: (A) experimental spectrum of the liquid; (B) calculated spectrum of the mixture of both conformers; (C) calculated spectrum of the axial conformer; and (D) calculated spectrum of the equatorial conformer.

i.e. the fundamentals at 879, 707 and 267 cm^{-1}. The mixing is not as extensive for the A″ modes but significant mixing is found for ν_{30}, ν_{31} and $\nu_{36}-\nu_{38}$. Similar mixing is also found for many of the corresponding modes of the axial conformer.

The structural parameters for the two conformers are remarkably similar. For the most part the heavy atom distances differ by 0.002 Å or less and the C–H distances are the same. Similarly, the angles differ by less than 1° for the corresponding ones between the two conformers. The puckering angle is the only one

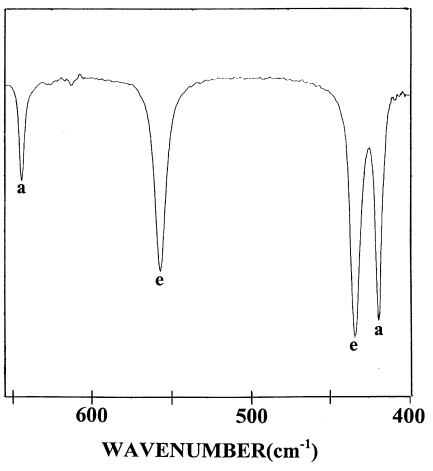

Fig. 7. Mid-infrared spectrum of cyclobutyl trifluorosilane dissolved in liquid krypton at −125°C.

that differs significantly between the two conformers with a 3.3° difference with the axial conformer having the smaller value of 28.34°. Since the parameters are nearly the same, the force constants are also expected to be nearly the same which, in fact, is the case. For this reason most of the corresponding fundamentals of the two conformers have nearly the same frequencies which made it difficult to obtain the enthalpy difference.

Acknowledgements

JRD would like to acknowledge partial support of these studies by the University of Missouri—Kansas City Faculty Research Grant program.

References

[1] J.R. Durig, L.A. Carreira, J.N. Willis, J. Chem. Phys. 57 (1972) 2755.
[2] J.R. Durig, A.D. Lopata, C.J. Wurrey, J. Raman Spectrosc. 3 (1975) 345.
[3] J.R. Durig, T.J. Geyer, T.S. Little, V.F. Kalasinsky, J. Chem. Phys. 86 (1987) 545.
[4] V.F. Kalasinsky, W.C. Harris, P.W. Holtzclaw, T.S. Little, T.J. Geyer, J.R. Durig, J. Raman Spectrosc. 18 (1987) 581.
[5] J.R. Durig, T.S. Little, M.J. Lee, J. Raman Spectrosc. 20 (1989) 757.
[6] J.R. Durig, M.J. Lee, T.S. Little, J. Raman Spectrosc. 21 (1990) 529.
[7] J.R. Durig, M.J. Lee, W. Zhao, T.S. Little, Struct. Chem. 3 (1992) 329.
[8] J.R. Durig, T.J. Geyer, M. Dakkouri, J. Phys. Chem. 89 (1985) 4307.
[9] M. Dakkouri, R. Bitschenauer, in preparation.
[10] M. Dakkouri, H. Kehrer, Chem. Ber. 116 (1983) 2041.
[11] F.A. Miller, B.M. Harney, Appl. Spectrosc. 24 (1970) 291.
[12] M.J. Frisch, G.W. Trucks, H.B. Schlegel, P.M.W. Gill, B.G. Johnson, M.A. Robb, J.R. Cheeseman, T.A. Keith, G.A. Petersson, J.A. Montgomery, K. Raghavachari, M.A. Al-Laham, V.G. Zakrzewski, J.V. Ortiz, J.B. Foresman, J. Cioslowski, B.B. Stefanov, A. Nanayakkara, M. Challacombe, C.Y. Peng, P.Y. Ayala, W. Chen, M.W. Wong, J.L. Andres, E.S. Replogle, R. Gomperts, R.L. Martin, D.J. Fox, J.S. Binkley, D.J. Defrees, J. Baker, J.P. Stewart, M. Head-Gordon, C. Gonzalez, J.A. Pople, GAUSSIAN 94 (revision B.3), Gaussian Inc., Pittsburgh, PA, 1995.
[13] P. Pulay, Mol. Phys. 17 (1969) 197.
[14] C. Moller, M.S. Plesset, Phys. Rev. 46 (1934) 618.
[15] J.H. Schachtschneider, Vibrational analysis of polyatomic molecules, Parts V and VI, Technical Report Nos. 231 and 57, Shell Development Co., Houston, TX, 1964 and 1965.
[16] M.J. Frisch, Y. Yamaguchi, J.F. Gaw, H.F. Schaefer III, J.S. Binkley, J. Chem. Phys. 84 (1986) 531.
[17] R.D. Amos, Chem. Phys. Lett. 124 (1986) 376.
[18] P.L. Polavarapu, J. Phys. Chem. 94 (1990) 8106.
[19] G.W. Chantry, in: A. Anderson (Ed.), The Raman Effect, 1, Marcel Dekker, New York, NY, 1971 Chapter 2.
[20] W.A. Herrebout, B.J. van der Veken, A. Wang, J.R. Durig, J. Phys. Chem. 99 (1995) 578.
[21] W.A. Herrebout, B.J. van der Veken, J. Phys. Chem. 100 (1996) 9671.
[22] M.O. Bulanin, J. Mol. Struct. 19 (1973) 59.
[23] M.O. Bulanin, J. Mol. Struct. 347 (1995) 73.
[24] B.J. van der Veken, F.R. DeMunck, J. Chem. Phys. 97 (1992) 3060.
[25] J.R. Durig, P.Q. Zhen, Y.P. Jin, T.K. Gounev, G.A. Guirgis, J. Mol. Struct. 477 (1999) 31.